Oxygen vacancies: The origin of *n*-type conductivity in ZnO

Lishu Liu,[1] Zengxia Mei,[1,*] Aihua Tang,[1] Alexander Azarov,[2] Andrej Kuznetsov,[2] Qi-Kun Xue,[3,†] and Xiaolong Du[1,‡]

[1]*Key Laboratory for Renewable Energy, Beijing National Laboratory for Condensed Matter Physics, Institute of Physics, Chinese Academy of Sciences, Beijing 100190, China*

[2]*Department of Physics, University of Oslo, Oslo P.O. Box 1048, NO-0316, Norway*

[3]*Department of Physics, Tsinghua University, Beijing 100084, China*

(Received 31 March 2016; revised manuscript received 24 May 2016; published 15 June 2016)

Oxygen vacancy (V_O) is a common native point defect that plays crucial roles in determining the physical and chemical properties of metal oxides such as ZnO. However, fundamental understanding of V_O is still very sparse. Specifically, whether V_O is mainly responsible for the *n*-type conductivity in ZnO has been still unsettled in the past 50 years. Here, we report on a study of oxygen self-diffusion by conceiving and growing oxygen-isotope ZnO heterostructures with delicately controlled chemical potential and Fermi level. The diffusion process is found to be predominantly mediated by V_O. We further demonstrate that, in contrast to the general belief of their neutral attribute, the oxygen vacancies in ZnO are actually +2 charged and thus responsible for the unintentional *n*-type conductivity as well as the nonstoichiometry of ZnO. The methodology can be extended to study oxygen-related point defects and their energetics in other technologically important oxide materials.

DOI: 10.1103/PhysRevB.93.235305

I. INTRODUCTION

Among metal oxides, ZnO is a prototypical *n*-type material with numerous applications, including catalysts, gas sensors, varistors, transparent electrodes, etc. Renewed interest has recently emerged for its ultraviolet light emission capabilities [1]. Progress towards ZnO-based optoelectronic devices and applications, however, has been impeded largely by unintentional and seemingly unavoidable *n*-type conductivity of ZnO materials that makes stable *p*-type doping extremely daunting. In order to solve this most puzzling problem for ZnO, it is highly desirable to understand the origin of the unintentional *n*-type conductivity [2–6].

It is generally accepted that the oxygen vacancy (V_O) plays a central role in determining the physical and chemical properties of metal oxides: it dominates various diffusion mechanisms involved in doping and its limitation, processing and device degradation, minority carrier lifetime, luminescence efficiency, etc. [7–13]. Specifically, V_O-related issues are of particular interest for ZnO. Whether the abovementioned *n*-type conductivity comes from V_O has remained a major problem in ZnO for a long time: O-deficient ZnO easily behaves as an *n*-type semiconductor even without the introduction of any intentional dopants [14]. Theoretical studies [15–17] seem consistently to indicate that V_O has the lowest formation enthalpy among the donorlike point defects. However, it leads to a deep electronic state in ZnO so that V_O could not be ionized and contribute to the conductivity at room temperature. The theoretically derived V_O defect energetics exhibit huge controversy probably owing to the finite-supercell formalism and the inaccurate description of the band structure of ZnO [18]: the formation enthalpy ΔH_f of neutral V_O under O-poor conditions ranges from −0.8 to 3.9 eV [15–17]. A formation enthalpy $\Delta H_f \geqslant 3.9$ eV as reported in Ref. [15] implies a V_O concentration $C(V_O) \leqslant 10^8$ cm^{-3}, which is far below the experimental value of 10^{17}–10^{19} cm^{-3} [19–21]. In the experimental side, most proposed models rely on some circumstantial methods and evidence [14,22]. Moreover, the charge state of V_O is much less addressed and remains as a controversial issue in ZnO.

To resolve these problems, we conduct a systematic study of oxygen self-diffusion in ZnO. Our paper employs a unique oxygen-isotope ZnO heterostructures with delicately controlled chemical potential (μ) and Fermi level (E_F). Unlike the gaseous-exchange technique, which has absorption and evaporation problems [23,24], the self-diffusion in the isotope heterostructures provides reliable information on the energetics and electronic properties of point defects [25–27]. We show unambiguously that the diffusion process of oxygen atoms in ZnO is predominantly mediated by V_O rather than oxygen interstitial (O_i). We further demonstrate that the oxygen vacancies in ZnO are +2 charged even near the conduction band minimum (CBM), in contrast to the general belief of their neutral attribute. The results establish that the oxygen vacancies are the dominant donorlike native point defects and thus responsible for the unintentional *n*-type conductivity as well as the nonstoichiometry of ZnO.

II. EXPERIMENTS

Oxygen-isotope samples were synthesized by radio-frequency plasma assisted molecular beam epitaxy (rf-MBE) on *c*-oriented sapphire substrate with several-nanometer-thick nitrided structure on the surface, and more nitridation pretreatment details can be found elsewhere [28]. The base pressure was in the range of 10^{-9} mbar. Two sorts of oxygen sources were used in the synthesis, one in its natural isotopic ratio (labeled as ^nO) and another one artificially enriched with ^{18}O isotope (>99.7%). A Zn^nO buffer layer was first deposited at 723 K, providing a good epitaxial template. Further, a Zn^nO epitaxial layer and an ^{18}O-enriched $Zn^{18}O$ layer were subsequently grown at 873 K. To realize the study of diffusion profiles as a function of μ, the Zn flux was varied for different

*zxmei@iphy.ac.cn
†qkxue@mail.tsinghua.edu.cn
‡xldu@iphy.ac.cn

 ©2016 American Physical Society

samples, while the radio-frequency power of the plasma gun and the flux of oxygen gas were kept constant at 300 W and 2.0 standard cubic centimeters (sccm), respectively. Specifically, the temperature of the Zn K-cell for Z1–Z5 is 605, 591, 585, 579, and 569 K, respectively. Thus, a series of isotopic heterostructures consisting of top $Zn^{18}O$ and bottom $Zn^{n}O$ were synthesized. It should be noted that the ^{18}O source used in the top $Zn^{18}O$ layer was mixed with 1.0 sccm artificially enriched ^{18}O (>99.7%) and 1.0 sccm ^{n}O, and the chemical potentials of Zn and O were, respectively, kept the same for the two different epilayers in each sample. Reflection high-energy electron diffraction (RHEED) was utilized *in situ* to monitor the whole epitaxial growth processes (see Fig. S1 in the Supplemental Material [29]).

Concentration depth profiles were measured by secondary ion mass spectroscopy (SIMS) using a Hiden MAXIM Analyser. For SIMS analysis, 5 keV Ar^{+} ions with a current 220 nA were used as a primary beam raster over an area of $200 \times 200\,\mu m^2$. The signal-to-concentration calibration was performed using standard ^{n}O and ^{18}O samples as a reference. The conversion of SIMS sputtering time-to-depth profiles was performed by measuring the crater depth using a Dektak 8 profilometer and assuming a constant erosion rate. Temperature-dependent Hall measurements were performed by the HL5500PC Hall Effect Measurement System.

III. RESULTS AND DISCUSSION

It is well known that the diffusion phenomenon is closely associated with the defect formation process. The defect formation enthalpy ΔH_f is given by

$$\Delta H_f(D^q,\mu,E_F) = E(D^q) - E_p + \mu + q(E_F + E_{VBM}), \quad (1)$$

where $E(D^q)$ is the total energy of the semiconductor with defect D in a charge state of q, and E_p is the energy of the perfect host. Here, μ, E_F, and E_{VBM} are the atomic chemical potential, the Fermi level, and the valence band maximum, respectively. Thus, the value of q, i.e., the charge state of a specific defect D^q, can be deduced from the dependence of ΔH_f on E_F.

To confirm the role of V_O in the n-type conductivity, the first thing is to determine whether and to what extent it is involved in the diffusion in the heterostructures. As can be seen from Eq. (1), ΔH_f is linearly related to μ [30], and will increase and decrease in V_O- and O_i-dominated diffusion processes, respectively, when μ moves towards O-rich conditions and the influence of E_F and other factors is negligible. For the experiments, a series of heterostructures consisting of top ^{18}O-enriched $Zn^{18}O$ and bottom natural $Zn^{n}O$ layers were thus obtained with different chemical potentials and the same Fermi levels, labeled as Z1, Z2, Z3, Z4, and Z5, respectively, as schematically illustrated in the inset of Fig. 1. The modulation of chemical potentials was realized through a gradually decreased Zn flux under a constant O flux. According to the growth rate, Z1 and Z2 can be regarded as Zn-rich samples, while Z3–Z5 are O-rich ones [31] (see Fig. S2 in the Supplemental Material [29]). The curves in Fig. 1 show the ^{18}O concentration depth profiles for the as-grown samples. The enriched $Zn^{18}O$ layers are immediately evident by the higher concentration of ^{18}O with respect to that in the bottom $Zn^{n}O$ layers. Interestingly, the ^{18}O profiles obviously become steeper when the μ moves towards O-rich conditions.

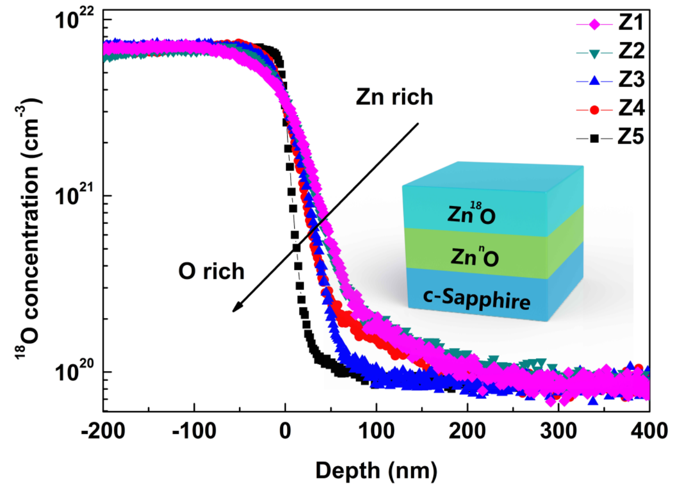

FIG. 1. ^{18}O concentration depth profiles in as-grown samples. Samples labeled as Z1 to Z5 were grown with decreased Zn/O ratio. The inset shows the schematic structure of these samples.

Annealing experiments were performed in a temperature range of 1023–1148 K for 30 min in vacuum. In order to ensure a fast ramping up to the desired diffusion temperature, the removable furnace was preheated and then moved to the sample place to perform the annealing process. The annealing temperatures were controlled within ±2 K. After annealing, the furnace was moved away immediately. According to the Fick's law, the self-diffusion profile of ^{18}O across an interface is described by [27]

$$C(x) = \frac{C_1 + C_2}{2} - \frac{C_1 - C_2}{2}\mathrm{erf}\left(\frac{x}{2\sqrt{Dt + k}}\right), \quad (2)$$

where $x = 0$ is at the interface, C_1 and C_2 are the initial ^{18}O concentrations at the top and bottom sides of the heterostructures, respectively, and erf(x) is the error function. The characteristic diffusion length is l ($l = 2\sqrt{Dt}$), where D is the self-diffusion coefficient (i.e., diffusivity) and t is the annealing time. A correction factor k is introduced in the fitting procedure owing to the initial distribution. The O self-diffusion coefficient D can be therefore derived based on Eq. (2). Figure 2(a) shows the typical ^{18}O concentration depth profiles of Z5 and their fitting curves as a function of annealing temperature using Eq. (2). The diffusion of ^{18}O atoms becomes more pronounced at elevated annealing temperature. As illustrated in Fig. 2(b), the samples with gradually varied chemical potentials show different profiles after annealing at 1073 K for 30 min. Note that D has a negatively exponential relation to the activation enthalpy ΔH_a, i.e., $D = D_o \exp(-\Delta H_a/k_B T)$, where D_o, k_B, and T denote the pre-exponential factor, Boltzmann constant, and temperature, respectively. Thus, using the data of D at different temperatures, the activation enthalpies ΔH_a can be obtained. Arrhenius plots of all of the extracted D values versus the

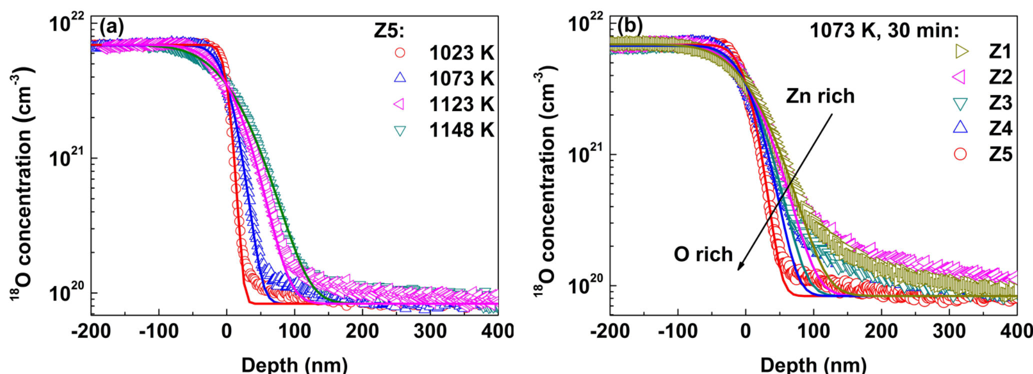

FIG. 2. Typical concentration depth profiles of ^{18}O after annealing in vacuum for 30 min. (a) Concentration depth profiles of ^{18}O with different annealing temperatures ranging from 1023 to 1148 K for Z5. The solid lines show the fitting results based on Eq. (2). (b) Concentration depth profiles of ^{18}O for Z1–Z5 after annealing at 1073 K for 30 min. The solid lines show the fitting results based on Eq. (2).

corresponding reciprocal absolute temperatures are presented in Fig. 3. As shown in Fig. 3, ΔH_a is 1.10 ± 0.04, 1.32 ± 0.05, 1.53 ± 0.04, 1.69 ± 0.03, and 2.56 ± 0.06 eV for Z1–Z5, respectively, when μ moves towards O-rich conditions.

It is well established that D is temperature dependent and affected by (i) the chemical potential μ (i.e., the partial pressures of Zn and O), (ii) the Fermi level E_{F}, and (iii) intentional or unintentional doping, i.e., externally controlled mechanism. To determine the dominant diffusion path in Z1–Z5, the influence of E_{F} and dopants on D has to be excluded first. In this case, D (and hence ΔH_a) will be more predominantly controlled by μ.

In our case, the carrier concentrations of Z1 to Z5 were obtained by temperature-dependent Hall measurements in vacuum from 473–823 K, and reached a nearly identical value, resulting in an almost constant E_{F} value in the range of 673–823 K (Fig. S3 in the Supplemental Material [29]). Note that E_{F} is estimated based on the well-known formula $E_{\mathrm{F}} = E_{\mathrm{F}}^i + k_{\mathrm{B}}T \ln(n_c/n_i)$, where E_{F}^i, n_c, and n_i denote Fermi level under the intrinsic condition, the carrier concentration, and the intrinsic carrier concentration, respectively. The temperature dependence of the band gap E_g is also taken into account in the above case [32]. The plots of E_{F} versus T are then reasonably extrapolated to the annealing temperature region in the diffusion experiments. As a result, an almost fixed E_{F} is obtained for the five samples Z1 to Z5, suggesting that the influence of E_{F} on the diffusion coefficient D can be neglected.

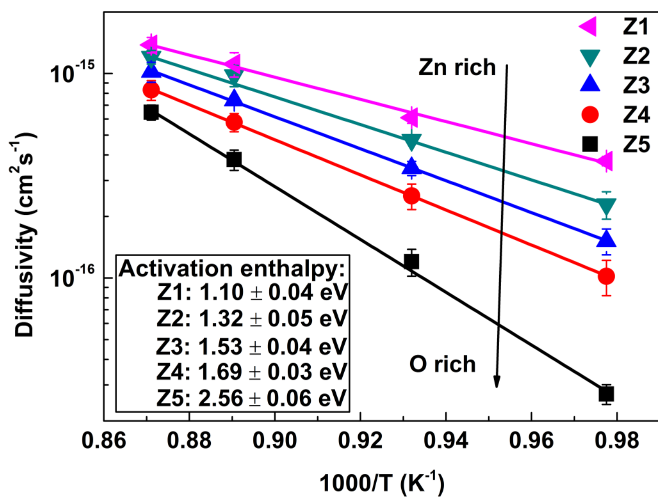

FIG. 3. Arrhenius plots of the extracted O self-diffusion coefficient D versus the reciprocal temperature 1000/T. The solid line shows the best fit to the self-diffusion coefficient. The inset shows the obtained activation enthalpy, which increases monotonically from Z1 (Zn rich) to Z5 (O rich).

Further, the defect concentrations can also be externally controlled, e.g., through intentional or unintentional doping. If impurity concentration is high enough, the dependence of D and ΔH_a on μ should be significantly less pronounced. However, for our samples, the diffusivity D increases by more than one order of magnitude when varying μ at 1023 K, as illustrated in Fig. 3. Moreover, the concentration of those unintentionally doped impurities is relatively low (Fig. S4 in the Supplemental Material [29]) so that their effect on D is negligible. As a result, the diffusivity D of the isotopic heterostructures Z1 to Z5 is primarily controlled by μ, which is the first goal of our experimental designs. Indeed, μ can control the defect concentrations and thus influence the diffusion process (see Supplemental Material [29]).

Under the assumption that the diffusion is a conventional point-defect-mediated process, the activation enthalpy ΔH_a of the diffusion defect species can be considered as the sum of the formation enthalpy ΔH_f and the migration enthalpy ΔH_m. The relatively low ΔH_a (1.10 ± 0.04 eV) for Z1 suggests that a direct diffusion mechanism without the need of forming thermally activated defects is more reasonable, namely the diffusing atoms simply jump into neighboring vacancy sites. Consequently, the activation enthalpy for Z1 is essentially determined by the migration enthalpy. For Z2 to Z5, on the other hand, the increased ΔH_a and lower D values at identical temperatures shown in Fig. 3 indicate that the defects of mediating diffusion are less favorable under O-rich conditions. In the case that only V_{O} and O_i are involved in diffusion, V_{O} should dominate the abovementioned self-diffusion process. Otherwise, if O_i is dominant, the trend for ΔH_a and D from Z1 to Z5 would be the opposite. Considering that the formation of V_{O}-V_{Zn} or V_{O}-O_i is independent of μ [33], the dominant defects are the isolated V_{O} rather than V_{O}-related complexes. Moreover, it is consistent with the monovacancy model, in which the migration enthalpy of vacancy ΔH_m^V is described

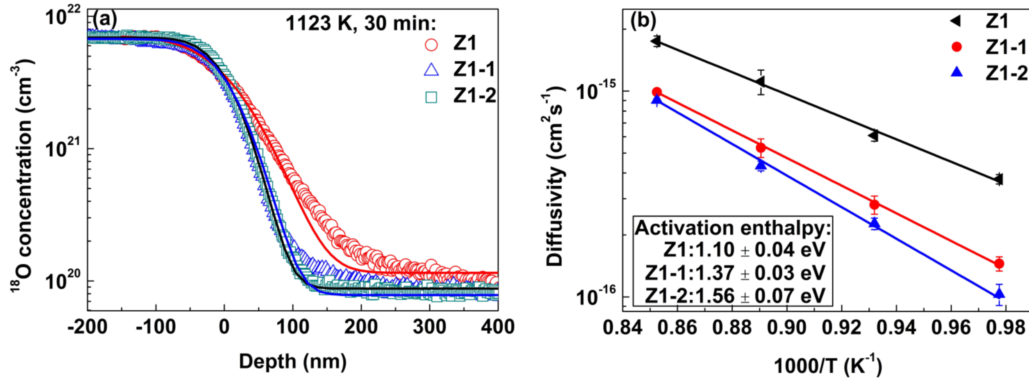

FIG. 4. (a) Concentration depth profiles of ^{18}O for samples with different E_F positions after annealing at 1123 K in vacuum for 30 min. (b) Extracted O self-diffusion coefficient D versus the reciprocal temperature 1000/T. The inset shows the obtained activation enthalpy, which increases from Z1 to Z1-2.

by [34,35]

$$\Gamma_O = \sqrt{\frac{8\Delta H_m^V}{3m\lambda^2}}, \tag{3}$$

where Γ_O, m, and λ represent the frequency of the highest vibrational mode in the crystal, the mass of O atom, and the lattice constant, respectively. Taking $\Gamma_O = 8 \times 10^{12}$ Hz [27,36] and $\lambda = 0.52$ nm [37] into account, we obtain $\Delta H_m^V = 1.08$ eV, which is in a good agreement with $\Delta H_a = 1.10 \pm 0.04$ eV for the Z1 sample (Fig. 3).

To figure out the dependence of ΔH_f on E_F and the charge state q of V_O, we investigate the influence of E_F on O diffusion. The modulation of E_F was achieved by effective Ga doping. Two more series of samples were studied. The first batch of samples Z1-1 and Z1-2 were grown using the conditions identical to those for Z1, except for *in situ* Ga doping contents of $\sim 2.0 \times 10^{18}$ cm^{-3} and $\sim 6.0 \times 10^{18}$ cm^{-3}, respectively (Fig. S5 in the Supplemental Material [29]). The second batch of samples Z2-1 and Z2-2 has Ga concentrations of $\sim 3.0 \times 10^{18}$ cm^{-3} and $\sim 1.5 \times 10^{19}$ cm^{-3}, respectively (Fig. S6 in the Supplemental Material [29]). Annealing experiments were performed in a temperature range of 1023–1173 K for these two batches of samples with modulated Fermi level. As illustrated in Fig. 4(a), the diffusion process is significantly retarded in Ga-doped samples. According to the Arrhenius plots in Fig. 4(b), the activation enthalpy ΔH_a increases from 1.10 ± 0.04 eV for the undoped sample Z1 to 1.56 ± 0.07 eV for the Ga-doped Z1-2. The ΔH_a for Z2, Z2-1, and Z2-2 shows similar behavior and increases from 1.32 ± 0.05 eV for Z2 to 1.77 ± 0.02 eV for Z2-2 (Fig. S7 in the Supplemental Material [29]). After annealing (up to 1173 K), the SIMS measurements do not reveal a significant redistribution of Ga compared to the as-grown samples (Fig. S8 in the Supplemental Material [29]), indicating that Ga dopant diffusion is negligible. Since the Zn/O ratio and thus μ are fixed for each batch of samples, the change in ΔH_a should be mainly attributed to the Fermi level change after Ga doping. Indeed, the Fermi level is below the CBM by 0.35, 0.18, and 0.12 eV [32] for undoped Z1 and Ga-doped Z1-1 and Z1-2 with carrier concentration of 1.0×10^{17} cm^{-3}, 1.0×10^{18} cm^{-3}, and 2.3×10^{18} cm^{-3}, respectively, at 823 K.

The result of the increased activation enthalpy with the upward Fermi level indicates that the dominant V_O is charged, which constitutes another finding of our paper. Since ΔH_f of charged defects is linearly related to E_F and ΔH_m is independent of E_F and μ for defects with a given state, ΔH_a is linearly dependent on E_F for defects with a given state. Accordingly, the slope of the $\Delta H_a - E_F$ curve gives the charge number q of the dominant defects [15]. The results for Z1 to Z1-2 and Z2 to Z2-2 are shown in Fig. 5. We can clearly see that ΔH_a increases with E_F, which is in contrast to the theory horizontal lines [15]. The fitting for both batches of samples gives a consistent value of q_1, $q_2 = +1.8$, indicating that the dominant V_O is +2 charged. Since the transition level from +2 to 0 is close to the CBM, the ionized V_O is a shallow donor and thus gives rise to the n-type conductivity in ZnO. The obtained $\Delta H_m = 1.10$ eV therefore corresponds to the migration barrier

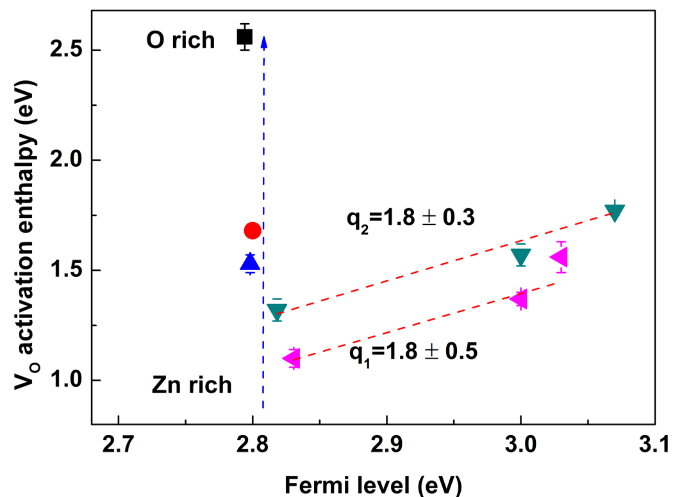

FIG. 5. Activation enthalpy of V_O as a function of Fermi level. Dashed lines illustrate an ascending trend for ΔH_a with increased Fermi level for two batches of samples: Z1 to Z1-2 and Z2 to Z2-2. As shown by the red dashed lines, the charged state of V_O is obtained by fitting the two batches of samples using linear relation, respectively. ΔH_a as a function of chemical potential is also included for Z1–Z5 samples, as illustrated by the blue dashed lines.

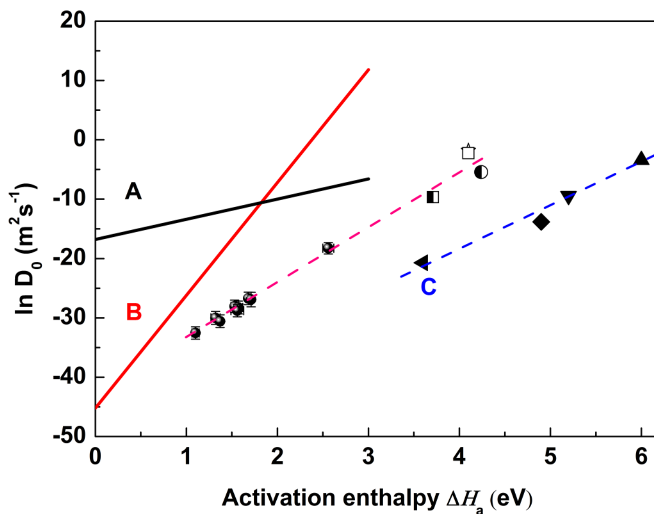

FIG. 6. The relationship between pre-exponential factor D_O and activation enthalpy ΔH_a. Also included are bulk metallic glasses (line A), crystalline metals (line B) [39] and results from self-diffusion in solids (line C): N in amorphous (◄) Si_3N_4 [40] and in polycrystalline Si_3N_4 (⧫) [41], Si in thermally grown SiO_2 (▼) [42], and infused SiO_2 (▲) [43]. The self-diffusion results from single crystalline solids are shown: N in GaN (☆) [44], O in ZnO (□) [45], and As (◧) [46] and Ga (◐) [27]) in GaAs. These dash lines show the trend.

for ∼+2 charged V_O, which is in excellent agreement with the theoretical result — 1.09 eV [36].

Further, the relationship between D_O and activation enthalpy ΔH_a is explored. Interestingly, as shown in Fig. 6, D_O increases as an exponential function of ΔH_a and can be expressed as $D_O = D_{OO} \exp(\Delta H_a/E_{MN})$, which is the so-called Meyer-Neldel law or compensation law [38]. The similar relation for bulk metallic glasses (line A) and crystalline metals (line B) is also included for comparison [39]. It is obvious that present results on ZnO are not in accordance with these two lines. Lower pre-exponential factor D_O occurs compared to those of A and B with a same activation enthalpy. It is also found for N in amorphous [40] and polycrystalline Si_3N_4 [41], Si in thermally grown SiO_2 [42], and infused SiO_2 [43] (labeled as line C). Notably, a striking similarity between Si_3N_4, SiO_2, and ZnO is the tetrahedrally coordinated bonding between cation and anion atoms. Considering the different crystalline situations between our samples and those from Refs. [40–43], i.e., single crystalline samples versus amorphous or polycrystalline ones, present results on ZnO are not in accordance with line C, but exhibit a similar trend. For N in GaN [44], O in ZnO [45], and As [46] or Ga [27] in GaAs, on the other hand, the published results are well consistent with our data. The straight line is often interpreted as an indication for a common or similar diffusion mechanism. Therefore, the tetrahedral structural units and crystalline situations were proposed playing a key role in the description of atomic motion in covalently bound solids [40].

IV. CONCLUSION

In conclusion, we have investigated the self-diffusion process of oxygen atoms as a function of μ and E_F in oxygen-isotopic ZnO heterostructures. It is found that V_O dominates the diffusion process with an activation enthalpy of 1.10–2.56 eV from Zn-rich to O-rich growth conditions. We have deduced the migration enthalpy to be 1.10 eV and found that the formation enthalpy of V_O increases even when E_F moves towards the CBM. Our results reveal that V_O is +2 charged even near the CBM, which is opposed to the usually believed neutral state. Our paper establishes oxygen vacancies as the dominant donorlike native point defects in ZnO and well explains the unintentional *n*-type conductivity, a mysterious problem in the last 50 years of study of ZnO. The methodology we have developed can be used to study oxygen-related point defects and their energetics in other technologically important metal oxides such as TiO_2 and In_2O_3, and thus is of general interest in the oxide and semiconductor physics community.

ACKNOWLEDGMENTS

This paper was supported by the Ministry of Science and Technology of China (Grants No. 2011CB302002 and No. 2011CB302006), the National Science Foundation of China (Grants No. 11174348, No. 51272280, No. 11274366, No. 61204067, No. 61306011, and No. 11321091), and the Research Council of Norway (Grant No. 221668).

[1] C. W. Litton, T. C. Collins, and D. C. Reynolds, *Zinc Oxide Materials for Electronic and Optoelectronic Device Applications* (John Wiley and Sons, Chichester, 2011).

[2] S. Lany and A. Zunger, Phys. Rev. B **72**, 035215 (2005).

[3] A. Janotti and C. G. Van de Walle, Nat. Mater. **6**, 44 (2007).

[4] C. G. Van de Walle, Phys. Rev. Lett. **85**, 1012 (2000).

[5] Y.-S. Kim and C. H. Park, Phys. Rev. Lett. **102**, 086403 (2009).

[6] D. C. Look, G. C. Farlow, P. Reunchan, S. Limpijumnong, S. B. Zhang, and K. Nordlund, Phys. Rev. Lett. **95**, 225502 (2005).

[7] M. Jochen and G. S. Darrell, Nature **430**, 620 (2004).

[8] R. Schaub, E. Wahlström, A. Rønnau, E. Lægsgaard, I. Stensgaard, and F. Besenbacher, Science **299**, 377 (2003).

[9] C. T. Campbell and C. H. F. Peden, Science **309**, 713 (2005).

[10] Z. Q. Liu, D. P. Leusink, X. Wang, W. M. Lü, K. Gopinadhan, A. Annadi, Y. L. Zhao, X. H. Huang, S. W. Zeng, Z. Huang, A. Srivastava, S. Dhar, T. Venkatesan, and Ariando, Phys. Rev. Lett. **107**, 146802 (2011).

[11] I. Grinberg, D. V. West, M. Torres, G. Gou, D. M. Stein, L. Wu, G. Chen, E. M. Gallo, A. R. Akbashev, P. K. Davies, J. E. Spanier, and A. M. Rappe, Nature **503**, 509 (2013).

[12] J. T. Mefford, W. G. Hardin, S. Dai, K. P. Johnston, and K. J. Stevenson, Nat. Mater. **13**, 726 (2014).

[13] P. Gao, Z. Kang, W. Fu, W. Wang, X. Bai, and E. Wang, J. Am. Chem. Soc. **132**, 4197 (2010).

[14] B. J. Jin, S. H. Bae, S. Y. Lee, and S. Im, Mater. Sci. Eng. B **71**, 301 (2000).

[15] A. Janotti and C. G. Van de Walle, Phys. Rev. B **76**, 165202 (2007).
[16] E.-C. Lee, Y.-S. Kim, Y.-G. Jin, and K. J. Chang, Phys. Rev. B **64**, 085120 (2001).
[17] S. Lany and A. Zunger, Phys. Rev. B **78**, 235104 (2008).
[18] S. J. Clark, J. Robertson, S. Lany, and A. Zunger, Phys. Rev. B **81**, 115311 (2010).
[19] L. E. Halliburton, N. C. Giles, N. Y. Garces, M. Luo, C. Xu, L. Bai, and L. A. Boatner, Appl. Phys. Lett. **87**, 172108 (2005).
[20] K. I. Hagemark, J. Electrochem. Soc. **122**, 992 (1975).
[21] F. Tuomisto, K. Saarinen, K. Grasza, and A. Mycielski, Phys. Status Solidi B **243**, 794 (2006).
[22] K. Dileep, L. S. Panchakarla, K. Balasubramanian, U. V. Waghmare, and R. Datta, J. Appl. Phys. **109**, 063523 (2011).
[23] G. W. Tomlins, J. L. Routbort, and T. O. Mason, J. Appl. Phys. **87**, 117 (2000).
[24] G. W. Tomlins and J. L. Routbort, J. Am. Ceram. Soc. **81**, 869 (1998).
[25] H. Bracht, S. P. Nicols, W. Walukiewicz, J. P. Silveira, F. Briones, and E. E. Haller, Nature **408**, 69 (2000).
[26] F. Strauß, L. Dörrer, T. Geue, J. Stahn, A. Koutsioubas, S. Mattauch, and H. Schmidt, Phys. Rev. Lett. **116**, 025901 (2016).
[27] L. Wang, L. Hsu, E. E. Haller, J. W. Erickson, A. Fischer, K. Eberl, and M. Cardona, Phys. Rev. Lett. **76**, 2342 (1996).
[28] Z. X. Mei, X. L. Du, Y. Wang, M. J. Ying, Z. Q. Zeng, H. Zheng, J. F. Jia, Q. K. Xue, and Z. Zhang, Appl. Phys. Lett. **86**, 112111 (2005).
[29] See Supplemental Material at http://link.aps.org/supplemental/10.1103/PhysRevB.93.235305 for additional graphs, a more detailed description of diffusion process and data tables.
[30] S. B. Zhang and J. E. Northrup, Phys. Rev. Lett. **67**, 2339 (1991).
[31] H.-J. Ko, T. Yao, Y. Chen, and S.-K. Hong, J. Appl. Phys. **92**, 4354 (2002).
[32] R. C. Rai, M. Guminiak, S. Wilser, B. Cai, and M. L. Nakarmi, J. Appl. Phys. **111**, 073511 (2012).
[33] R. Vidya, P. Ravindran, H. Fjellvåg, B. G. Svensson, E. Monakhov, M. Ganchenkova, and R. M. Nieminen, Phys. Rev. B **83**, 045206 (2011).
[34] A. Seeger and K. P. Chik, Phys Status Solidi **29**, 455 (1968).
[35] R. Kube, H. Bracht, E. Hüger, H. Schmidt, J. L. Hansen, A. N. Larsen, J. W. Ager, E. E. Haller, T. Geue, and J. Stahn, Phys. Rev. B **88**, 085206 (2013).
[36] P. Erhart and K. Albe, Phys. Rev. B **73**, 115207 (2006).
[37] E. H. Kisi and M. M. Elcombe, Acta Crystallogr C **45**, 1867 (1989).
[38] W. Meyer and H. Neldel, Z. Tech. Phys. **12**, 588 (1937).
[39] F. Faupel, W. Frank, M.-P. Macht, H. Mehrer, V. Naundorf, K. Rätzke, H. R. Schober, S. K. Sharma, and H. Teichler, Rev. Mod. Phys. **75**, 237 (2003).
[40] H. Schmidt, M. Gupta, and M. Bruns, Phys. Rev. Lett. **96**, 055901 (2006).
[41] H. Schmidt, G. Borchardt, M. Rudolphi, H. Baumann, and M. Bruns, Appl. Phys. Lett. **85**, 582 (2004).
[42] T. Takahashi, S. Fukatsu, K. M. Itoh, M. Uematsu, A. Fujiwara, H. Kageshima, Y. Takahashi, and K. Shiraishi, J. Appl. Phys. **93**, 3674 (2003).
[43] G. Brebec, G. Seguin, C. Sella, J. Bevenot, and J. C. Martin, Acta Metall. **28**, 327 (1980).
[44] O. Ambacher, F. Freudenbeag, R. Dimitrov, H. Angerer, and M. Stutzmann, Jpn. J. Appl. Phys. **37**, 2416 (1998).
[45] J. W. Hoffman and I. Lauder, Trans. Faraday Soc. **66**, 2346 (1970).
[46] G. Bösker, J. Pöpping, N. A. Stolwijk, H. Mehrer, and A. Burchard, Hyperfine Interact. **129**, 337 (2000).